Computing the quasinormal modes and eigenfunctions for the Teukolsky equation using horizon penetrating, hyperboloidally compactified coordinates

Justin L. Ripley

DAMTP, Centre for Mathematical Sciences, University of Cambridge, Wilberforce Road, Cambridge CB3 0WA, UK.

E-mail: `jr860@cam.ac.uk`

June 2022

Abstract. We study the quasinormal mode eigenvalues and eigenfunctions for the Teukolsky equation in a horizon penetrating, hyperboloidally compactified (HPHC) coordinate system. Following earlier work by Zenginoğlu [1], we show that the quasinormal eigenfunctions for the Teukolsky equation are regular from the black hole horizon to future null infinity in these coordinates. We then present several example quasinormal eigenfunction solutions, and study some of their properties in the near-extremal Kerr limit.

keywords: black holes, quasinormal modes, quasinormal eigenfunctions, hyperboloidal compactification

1. Introduction

The Teukolsky equation describes the dynamics of linear spin s fields on the Kerr black hole spacetime [2]. As this equation describes an inherently dissipative system (waves can fall into the black hole, or propagate to future null infinity), the Teukolsky equation does not have mode solutions, but instead has *quasi*normal mode solutions. In this work we will be interested in computing not just the quasinormal modes (QNMs) of the Teukolsky equation, but also the quasinormal *eigenfunction* (QNEs) associated with each mode.

The QNMs of the Teukolsky equation have found use in astrophysics, theoretical physics, and mathematical relativity [3, 4, 5, 6]. Teukolsky QNM mode calculations are typically computed using coordinates where the constant time hypersurfaces intersect the bifurcation sphere and spatial infinity (for example Boyer-Lindquist coordinates have this property [7]) [2, 8, 9, 10, 11]. As was pointed out though by Zenginoğlu, horizon-penetrating, hyperboloidally compactified (HPHC) coordinates–that is, coordinates where constant time hypersurfaces intersect both the black hole horizon and future null infinity (see Fig. 1)–can be considered a more "natural" set of coordinates to study black hole perturbations [1]. This is because in HPHC coordinates, on constant time hypersurfaces the QNEs are regular at the horizon and at future null infinity‡. By contrast, on constant time hypersurfaces the QNEs blow up exponentially at the bifurcation sphere and at spatial infinity. Moreover, a timelike observer can never reach the bifurcation sphere or spatial infinity, so from a physical perspective it is not necessary to know how the QNEs behave near those two locations. Here we extend and complete the calculations begun in [1], by computing the QNMs and QNEs for the Kerr black hole in HPHC coordinates§ We use a spectral/pseudospectral method to compute the QNEs.

Recently the *pseudospectrum* of the QNMs of Schwarzschild black holes [17] and Reissner-Nordstrom black holes [18] were computed in HPHC coordinates. The pseudospectrum of a mode solution roughly captures how sensitive the solution is to perturbations of the underlying equation of motion [19]. In this sense, the pseudospectrum of the Teukolsky equation then quantifies the stability of QNMs to perturbations of the underlying Kerr spacetime‖. Computing the pseudospectrum requires evaluating QNEs in a suitable norm, which is one reason why HPHC coordinates were used in [17, 18]: in these coordinates the QNEs remain finite over the entire exterior of the black hole, which makes finding a well-behaved norm relatively straightforward.

‡ Press and Teukolsky were the first to note that the QNEs of the Teukolsky equation do not blow up at the black hole horizon when one works with an appropriate tetrad in horizon penetrating coordinates, and that the QNEs do not blow up at future null infinity if one works in outgoing coordinates [12].
§ In contrast to calculations of QNEs, which are computed in the frequency domain, there has several works that compute the evolution of the Teukolsky equation in the time domain using HPHC coordinates [13, 14, 15, 16].
‖ For other recent attempts to investigate the stability of the quasinormal mode solutions to the Teukolsky equation; see [20, 16, 21, 22].
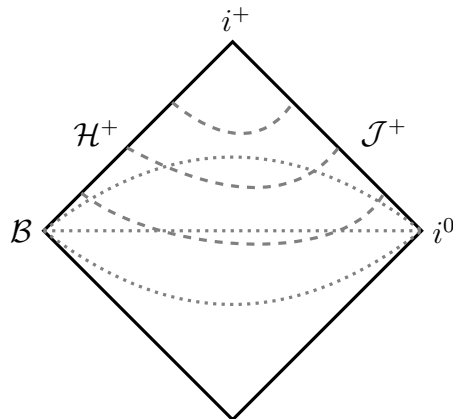
Figure 1. Schematic Penrose diagram of the Kerr black hole spacetime exterior to the future horizon that illustrates the horizon-penetrating, hyperboloidally compactified coordinates used in this article. The dotted lines describe $t = const.$ hypersurfaces in Boyer-Lindquist coordinates, while the dashed lines describe $\tau = const.$ hypersurfaces in the horizon-penetrating, hyperboloidally compactified coordinates we use. Here $\mathcal{H}^+$ is the future black hole horizon, $\mathcal{J}^+$ is future null infinity, i^+ is future timelike infinity, i^0 is spacelike infinity, and $\mathcal{B}$ is the bifurcation sphere of the black hole.

This work is partly motivated by the pseudospectral research program initiated in [17, 18], as (to our knowledge) no equivalent computation of the QNEs of the Teukolsky equation in HPHC coordinates has yet been completed.

This note is organized as follows. We first derive the Teukolsky equation in HPHC coordinates, and separate the resulting equation into two ordinary differential equations (ODEs). We use of a spectral method to discretize the angular equation, and a pseudospectral method to discretize the radial equation. We then present a method to numerically compute the QNMs and QNEs of the Teukolsky equation by rephrasing the two discretized ODEs as a joint eigenvalue problem. We present some example QNE solutions, and study their functional form in the (near) extremal limit $a \to M$. In the appendices we provide a code comparison of our code to the `qnm` code [23], present a convergence study of an example QNE solution, and review some properties of orthogonal polynomials which we make use of in our (pseudo)spectral code.

The metric signature is $-+++$, and we set $G = c = \hbar = 1$. The real and imaginary part of a number are denoted by $\mathcal{R}$ and $\mathcal{I}$, respectively.

Our code is available online [24].

2. Hyperboloidal compactification of the Teukolsky equation

We first rewrite the Teukolsky equation in a HPHC coordinate system. Our general approach follows [16]; see also [1, 25, 26] for other potential choices of HPHC coordinates. The Teukolsky equation in Boyer-Lindquist coordinates is [2]

$$\left[\frac{(r^2 + a^2)^2}{\Delta} - a^2 \sin^2 \theta \right] \partial_t^2 \psi - \Delta^{-s} \partial_r \left(\Delta^{s+1} \partial_r \psi \right) + \frac{4Mar}{\Delta} \partial_t \partial_\varphi \psi + \frac{a^2}{\Delta} \partial_\varphi^2 \psi - {}_s\!\!\not\!\Delta \psi$$

$$-2s\frac{a(r-M)}{\Delta}\partial_\varphi\psi - 2s\left[\frac{M\left(r^2-a^2\right)}{\Delta} - r - ia\cos\theta\right]\partial_t\psi = 0, \tag{1}$$

where M is the black hole mass, a is the black hole spin, and s is the spin of the wave (± 2 for gravity, ± 1 for electromagnetism, etc). The spin-weighted spherical Laplacian is

$$_s\!\!\not\!\Delta\psi \equiv \frac{1}{\sin\theta}\partial_\theta\left(\sin\theta\partial_\theta\psi\right) + \left(s - \frac{\left(-i\partial_\varphi + s\cos\theta\right)^2}{\sin^2\theta}\right)\psi. \tag{2}$$

We also have used the standard notation

$$\Delta \equiv r^2 - 2Mr + a^2. \tag{3}$$

The zeros of Δ determine the location of the inner and outer horizons:

$$r_\pm \equiv M \pm \sqrt{M^2 - a^2}. \tag{4}$$

We transform to ingoing coordinates by defining the variables

$$dv \equiv dt + \frac{2Mr}{\Delta}dr, \qquad d\phi \equiv d\varphi + \frac{a}{\Delta}dr. \tag{5}$$

We also radially rescale ψ to make the Teukolsky equation regular at the horizon, and to remove the "long-range potential" in the Teukolsky equation [27, 28]

$$\psi \equiv \frac{1}{r}\Delta^{-s}\Psi. \tag{6}$$

The Teukolsky equation now reads

$$\left(r^2 + 2Mr + a^2\cos^2\theta\right)\partial_v^2\Psi - 4Mr\partial_v\partial_r\Psi - \Delta\partial_r^2\Psi - 2a\partial_r\partial_\phi\Psi - {}_s\!\!\not\!\Delta\Psi$$

$$+2\left[M + s\left(M + r + ia\cos\theta\right)\right]\partial_v\Psi + 2\left[-M + \frac{a^2}{r} + s\left(r - M\right)\right]\partial_r\Psi + \frac{2a}{r}\partial_\phi\Psi$$

$$+2\left(\frac{sM}{r} + \frac{Mr - a^2}{r^2}\right)\Psi = 0. \tag{7}$$

We next transform the time variable to achieve a hyperboloidal slicing of the spacetime; this will make the Teukolsky equation regular at future null infinity [25, 1]. We define the hyperboloidal time variable τ

$$d\tau \equiv dv + \frac{dh}{dr}dr, \tag{8}$$

where $h(r)$ is a "height" function designed so that the radially ingoing characteristic speed is zero at $r = \infty$. Ultimately we find

$$\frac{dh}{dr} = -1 - \frac{4M}{r}, \tag{9}$$

to be a suitable height function [25, 26, 16]. We choose the radial compactification

$$\rho \equiv \frac{1}{r}, \tag{10}$$

so $r = \infty$ is located at $\rho = 0$. The Teukolsky equation now reads

$$\left[16M^2 - a^2 \sin^2\theta + 8M\left(4M^2 - a^2\right)\rho - 16a^2M^2\rho^2\right]\partial_\tau^2\Psi - \rho^4\Delta\partial_\rho^2\Psi - {}_s\!\!\not{\!\Delta}\Psi$$
$$-2\left[1 + \left(a^2 - 8M^2\right)\rho^2 + 4a^2M\rho^3\right]\partial_\tau\partial_\rho\Psi + 2a\rho^2\partial_\rho\partial_\phi\Psi + 2a\left(1 + 4M\rho\right)\partial_\tau\partial_\phi\Psi$$
$$+2\left[s\left(-2M + ia\cos\theta\right) + \left(4M^2\left\{s+2\right\} - a^2\right)\rho - 6Ma^2\rho^2\right]\partial_\tau\Psi$$
$$+2\left[-1 - s + (s+3)M\rho - 2a^2\rho^2\right]\rho\partial_\rho\Psi + 2a\rho\partial_\phi\Psi$$
$$+2\left(Ms + M - a^2\rho\right)\rho\Psi = 0. \tag{11}$$

The Teukolsky equation remains regular at the radial endpoints $\rho = 0, \rho = \rho_+$ (although it is still singular at $\theta = 0, \pi$). At future null infinity (located at $\rho = 0$), the radial ingoing characteristic speed is zero.

For reference, and to verify that $\rho = 0$ limits to an asymptotically flat spacetime, we next present the Kerr line element in the coordinates $\{\tau, r \equiv 1/\rho, \theta, \phi\}$. Defining $\Sigma \equiv r^2 + a^2\cos^2\theta$, the line element is:

$$ds^2 = -\left(1 - \frac{2Mr}{\Sigma}\right)d\tau^2 + 8M\frac{1}{\Sigma}\left(1 + \frac{2M}{r}\right)\left(2M - \frac{a^2}{r}\cos^2\theta\right)dr^2$$
$$-2\left(1 + \frac{4M}{r} - \frac{4M\left(r + 2M\right)}{\Sigma}\right)d\tau dr - 4a\frac{Mr}{\Sigma}\sin^2\theta d\tau d\phi$$
$$-2a\left(1 + 4M\frac{r + 2M}{\Sigma}\right)\sin^2\theta dr d\phi + \Sigma d\theta^2 + \left(a^2 + r^2 + 2Mr\frac{a^2}{\Sigma}\sin^2\theta\right)\sin^2\theta d\phi^2. \tag{12}$$

Holding $\tau = const., \theta = const.,$ and $\phi = const.,$ the radial proper distance line element dr_p is

$$dr_p = 8M\frac{1}{\Sigma}\left(1 + \frac{2M}{r}\right)\left(2M - \frac{a^2}{r}\cos^2\theta\right)dr. \tag{13}$$

This is finite and bounded for all $r_+ < r < \infty$, thus we see that the proper radial distance from any point $r_+ < r_0 < \infty$ to the black hole horizon is always bounded, including in the extremal limit $a/M \to 1$. In the limit $r \to \infty$, the metric is flat, including in the extremal limit [25, 26]

$$\lim_{r\to\infty} ds^2 = -d\tau^2 - 2d\tau dr + r^2\left(d\theta^2 + \sin^2\theta d\phi^2 + \mathcal{O}\left(\frac{1}{r^2}\right)\right) + \mathcal{O}\left(1\right)dr d\phi. \tag{14}$$

To summarize: we see that we have chosen coordinates so that on $\tau = const.$ hypersurfaces, even in the limit $a/M \to 1$, $r = \infty$ $(\rho = 0)$ corresponds to future null infinity, $r = r_+$ $(\rho = \rho_+)$ corresponds to the black hole horizon, and the proper radial distance to the black hole horizon remains bounded.

3. Quasinormal mode solutions to the Teukolsky equation

3.1. Separating the Teukolsky equation into ODEs

To determine the quasinormal modes and eigenfunctions of the Teukolsky equation, we first apply separation of variables [2]

$$\Psi\left(\tau, \rho, \theta, \phi\right) = e^{-i\omega\tau + im\phi}R(\rho)S(\theta). \tag{15}$$

With this, the Teukolsky equation separates into a radial and an angular equation:

$$-\rho^2 \hat{\Delta}(\rho) \frac{d^2 R}{d\rho^2} + A(\omega, m, \rho) \frac{dR}{d\rho} + (B(\omega, m, \rho) - {}_s\Lambda_l^m) R = 0, \tag{16}$$

$$\frac{1}{\sin\theta} \frac{d}{d\theta} \left(\sin\theta \frac{dS}{d\theta} \right) + \left(s - \frac{(m + s\cos\theta)^2}{\sin^2\theta} - 2a\omega s\cos\theta + a^2\omega^2\cos^2\theta + {}_s\Lambda_l^m \right) S = 0. \tag{17}$$

We have defined

$$\hat{\Delta}(\rho) \equiv 1 - 2M\rho + a^2\rho^2, \tag{18}$$

$$A(\omega, m, \rho) \equiv 2i\omega - 2(1+s)\rho + 2\left[i\omega\left(a^2 - 8M^2\right) + ima + (s+3)M \right]\rho^2$$
$$+ 4\left[2i\omega M - 1\right]a^2\rho^3, \tag{19}$$

$$B(\omega, m, \rho) \equiv \left(a^2 - 16M^2\right)\omega^2 + 2(ma + 2isM)\omega$$
$$+ 2\left[4\left(a^2 - 4M^2\right)M\omega^2 + \left(4maM - 4i(s+2)M^2 + ia^2\right)\omega + ima + (s+1)M\right]\rho$$
$$+ 2\left(8M^2\omega^2 + 6iM\omega - 1\right)a^2\rho^2. \tag{20}$$

The separation constant ${}_s\Lambda_l^m$ can be thought of as a function of $a\omega$. The radial equation has regular singular points at the two zeros of Δ and at $\rho = \infty$ ($r = 0$), and an irregular singular point at $\rho = 0$ ($r = \infty$).

3.2. Solution to the radial ODE near future null infinity and near the black hole horizon

We next show that the ingoing (into the domain) wave solutions near future null infinity ($\rho \sim 0$) and near the black hole horizon ($\rho \sim \rho_+$) are not smooth at those boundary points. We also show that smooth solutions to the radial ODE represent outgoing/stationary waves at the horizon and future null infinity. Our notation for the (confluent) hypergeometric function will follow [29]; see also [30] for a general reference.

First we consider the behavior of solutions near $\rho = 0$ (the irregular singular point of Eq. 16). To leading order in ρ we have a confluent hypergeometric equation

$$-\rho^2 \frac{d^2 R_{\mathcal{J}}}{d\rho^2} + [2i\omega - 2(1+s)\rho] \frac{dR_{\mathcal{J}}}{d\rho}$$
$$+ \left[\left(a^2 - 16M^2\right)\omega^2 + 2(ma + 2isM)\omega - {}_s\Lambda_l^m\right] R_{\mathcal{J}} = 0. \tag{21}$$

The general solution to this equation is [29]

$$R_{\mathcal{J}}(\rho) = \left(-\frac{2i\omega}{\rho}\right)^{a_{\mathcal{J}}} \left[\mathcal{A}_{\mathcal{J}} \times M\left(a_{\mathcal{J}}, c_{\mathcal{J}}; -\frac{2i\omega}{\rho}\right) + \mathcal{B}_{\mathcal{J}} \times U\left(a_{\mathcal{J}}, c_{\mathcal{J}}; -\frac{2i\omega}{\rho}\right)\right], \tag{22}$$

where $\mathcal{A}_{\mathcal{J}}, \mathcal{B}_{\mathcal{J}}$ are constants, M, U are respectively the confluent hypergeometric functions of the first and second kind, and

$$a_{\mathcal{J}} \equiv \frac{1}{2}\left(1 + 2s - \sqrt{4c + (1+2s)^2}\right), \tag{23}$$

$$c_{\mathcal{J}} \equiv 1 - \left(4\left[\left(a^2 - 16M^2\right)\omega^2 + 2(ma + 2isM)\omega - {}_s\Lambda_l^m\right]^2 + (1+2s)^2\right)^{1/2}. \tag{24}$$

In the limit $\rho \to 0$, the limiting solution to the function multiplied by $\mathcal{A}_{\mathcal{J}}$ is (here we have reintroduced the harmonic time dependence)

$$\lim_{\rho \to 0} e^{-i\omega\tau} \left(-\frac{2i\omega}{\rho}\right)^{a_{\mathcal{J}}} M\left(a_{\mathcal{J}}, c_{\mathcal{J}}; -\frac{2i\omega}{\rho}\right) \sim \left(-\frac{2i\omega}{\rho}\right)^{a_{\mathcal{J}}} \exp\left(-i\omega\tau - \frac{2i\omega}{\rho}\right) (\cdots). \quad (25)$$

This describes a wave solution that is ingoing into the computational domain, and we see that it is irregular as $\rho \to 0$. To remove the ingoing wave solution we then set $\mathcal{A}_{\mathcal{J}} = 0$. The solution then reads

$$R_{\mathcal{J}}(\rho) = \mathcal{B}_{\mathcal{J}} \times \left(-\frac{2i\omega}{\rho}\right)^{a_{\mathcal{J}}} U\left(a_{\mathcal{J}}, c_{\mathcal{J}}; -\frac{2i\omega}{\rho}\right). \quad (26)$$

As the limiting behavior of confluent hypergeometric function of the second kind is

$$\lim_{\rho \to 0} U\left(a_{\mathcal{J}}, c_{\mathcal{J}}; -\frac{2i\omega}{\rho}\right) \sim \left(-\frac{2i\omega}{\rho}\right)^{-a_{\mathcal{J}}} (\cdots), \quad (27)$$

we see that this solution near future null infinity goes as

$$\lim_{\rho \to 0} e^{-i\omega\tau} R_{\mathcal{J}}(\rho) \sim e^{-i\omega\tau} \times (const. + \mathcal{O}(\rho)). \quad (28)$$

From Eq. 28, we see that the solution Eq. 26 does not support mode solutions that are ingoing into the computational domain near $\rho = 0$. At "worst" it supports modes that are neither ingoing nor outgoing, which are consistent with ingoing waves that live exactly at future null infinity; i.e. modes that have support exactly at $\rho = 0$.

We next show that near the black hole horizon ($\rho \sim \rho_+ \equiv 1/r_+$), there are two solutions, one of which is regular and one which is irregular at $\rho = 0$. Furthermore we show that the irregular solution describes an ingoing wave solution, and the regular solution describes and outgoing/stationary wave solution.

To leading order in $x \equiv (1 - \rho/\rho_+)$, the radial ODE reduces to a hypergeometric equation:

$$x(\sigma + x)\frac{d^2 R_{\mathcal{H}}}{dx^2} + \left[\frac{\rho_-}{\rho_+^2} A(\omega, m, \rho_+) - \left(\frac{\rho_-}{\rho_+}\frac{dA}{d\rho}\bigg|_{\rho=\rho_+}\right)x\right]\frac{dR_{\mathcal{H}}}{dx}$$

$$-\frac{\rho_-}{\rho_+}\left(B(\omega, m, \rho_+) - {}_s\Lambda_l^m\right)R_{\mathcal{H}} = 0, \quad (29)$$

where $\sigma \equiv (\rho_-/\rho_+ - 1)$. Generally we can write the near-horizon solution as

$$R_{\mathcal{H}}(x) = \mathcal{A}_{\mathcal{H}} \times F\left(a_{\mathcal{H}}, b_{\mathcal{H}}, \frac{c_{\mathcal{H}}}{\sigma}; -\frac{x}{\sigma}\right)$$

$$+ \mathcal{B}_{\mathcal{H}} \times \left(\frac{x}{\sigma}\right)^{1 - c_{\mathcal{H}}/\sigma} F\left(1 + a_{\mathcal{H}} - \frac{c_{\mathcal{H}}}{\sigma}, 1 + b_{\mathcal{H}} - \frac{c_{\mathcal{H}}}{\sigma}, 2 - \frac{c_{\mathcal{H}}}{\sigma}; -\frac{x}{\sigma}\right), \quad (30)$$

where $\mathcal{A}_{\mathcal{H}}, \mathcal{B}_{\mathcal{H}}$ are constants, F is the hypergeometric function, and

$$c_{\mathcal{H}} \equiv \frac{\rho_-}{\rho_+^2}\left(2\left(1 + \left(a^2 - 8M^2\right)\rho_+^2 + 4Ma^2\rho_+^3\right)i\omega\right.$$

$$\left. -2(1+s)\rho_+ + 2\left[ima + (s+3)M\right]\rho_+^2 - 4a^2\rho_+^3\right) \quad (31)$$

$$1 + a_{\mathcal{H}} + b_{\mathcal{H}} \equiv \frac{\rho_-}{\rho_+} \Bigg(\left(-24a^2 M \rho_+^2 - 4a^2 \rho_+ + 32M^2 \rho_+ \right) i\omega$$

$$+ 2\left(1 + s\right) + 12a^2 \rho_+^2 - 4ima\rho_+ - 4\left(3 + s\right) M\rho_+ \Bigg), \tag{32}$$

$$a_{\mathcal{H}} b_{\mathcal{H}} \equiv - \left(\left(a^2 - 16M^2 \right) \omega^2 + 2\left(ma + 2isM \right) \omega \right) \frac{\rho_-}{\rho_+}$$

$$-2 \left[4\left(a^2 - 4M^2 \right) M\omega^2 + 4\left(maM - i\left(s + 2 \right) M^2 + ia^2 \right) \omega + ima + \left(s + 1 \right) M \right] \rho_-$$

$$-2 \left(8a^2 M^2 \omega^2 + 6ia^2 M\omega - a^2 \right) \rho_+ \rho_-., \tag{33}$$

Near $x \sim 0$, the term multiplied by $\mathcal{B}_{\mathcal{H}}$ goes as (here we have reintroduced the harmonic time dependence)

$$\sim \mathcal{B}_{\mathcal{H}} \times \exp\left[-i\omega\tau + \left(\frac{c_{\mathcal{H}}}{\sigma} - 1 \right) \log\frac{\sigma}{x} \right] (\cdots). \tag{34}$$

We see that this solution describes waves that oscillate rapidly near $x = 0$, and are ingoing into the computational domain provided the component $c_{\mathcal{H}}/\sigma - 1$ which multiplies $i\omega$ is negative. Examining

$$\frac{c_{\mathcal{H}}}{\sigma} - 1 = \left(\frac{2}{\sigma} \frac{\rho_-}{\rho_+^2} \left(1 + \left(a^2 - 8M^2 \right) \rho_+^2 + 4Ma^2 \rho_+^3 \right) \right) i\omega + \cdots, \tag{35}$$

and noting that $\rho_-, \rho_+, \sigma \geq 0$, we see that we only need to determine if $\left(1 + \left(a^2 - 8M^2 \right) \rho_+^2 + 4Ma^2 \rho_+^3 \right)$ is negative. Using $\rho_+ \equiv 1/r_+ = 1/(M + \sqrt{M^2 - a^2})$, it is straightforward to verify that this is true for all $a \in [0, M]$. Thus 34 describes an ingoing mode solution. The regular solution limits to a constant as $x \to 0$:

$$\mathcal{R}_{\mathcal{H}} = \mathcal{A}_{\mathcal{H}} \times F\left(a_{\mathcal{H}}, b_{\mathcal{H}}, \frac{c_{\mathcal{H}}}{\sigma}; -\frac{x}{\sigma} \right) = \mathcal{A}_{\mathcal{H}} + \mathcal{O}\left(x \right). \tag{36}$$

Similar to the regular solution at $\rho = 0$ (Eq. 26), we see that the solution Eq. 36 does not support mode solutions that are ingoing into the computational domain. At "worst" it supports modes that are neither ingoing nor outgoing, which are consistent with outgoing waves that live exactly at the black hole horizon; i.e. support exactly at $\rho = \rho_+$.

To conclude, we have shown that the radial Teukolsky equation admits a regular and an irregular solution at the two boundary points $\rho = 0, \rho_+$. We have shown that the irregular solutions represent modes which are ingoing into the computational domain, while the regular solutions do not support such modes. Thus the physical boundary conditions for the radial equation are to impose regularity at $\rho = 0, \rho_+$.

4. Discretization of the angular and radial ODEs, and numerically computing the quasinormal modes

We discretize the radial equation, Eq. 16, using Chebyshev pseudospectral (collocation) methods (e.g. [31, 32]). These methods automatically impose regularity of the solution

at the boundaries of the domain $\rho = 0, \rho_+$¶. We briefly review Chebyshev pseudospectral methods in Appendix C.

We discretize the angular equation, Eq. 17, using a spectral method [34] (see also Appendix A of [35]). We expand the spin-weighted spheroidal harmonics as a linear sum of spin-weighted spherical harmonics, and evaluate the angular ODE in coefficient/spectral space. In spectral space the angular ODE reduces to a sparse, banded matrix equation. For completeness, we briefly review this method in Appendix B.

Fixing the labels (s, l, m), the discretized radial and angular ODEs respectively take the form

$$\sum_{j=0}^{N_{(\rho)}} \left(\left[\hat{M}_{(\rho)}(\omega) \right]_{ij} - \Lambda_{(\rho)} \hat{I}_{ij} \right) \vec{f}_j = 0, \tag{37}$$

$$\sum_{j=0}^{N_{(\theta)}} \left(\left[\hat{M}_{(\theta)}(\omega) \right]_{ij} - \Lambda_{(\theta)} \hat{I}_{ij} \right) \vec{g}_j = 0. \tag{38}$$

The matrices $\hat{M}_{(\rho)}$ and $\hat{M}_{(\theta)}$ are functions of powers of ρ, ω as can be seen respectively from Eq. 16 and Eq. 17, and $\Lambda_{(\rho/\theta)}$ are the separation constants $_s\Lambda_l^m(a\omega)$. We view the system Eq. 37, Eq. 38 as an eigenvalue equation for the angular separation constant: the QNMs are the ω such that $\Lambda_{(\rho)} = \Lambda_{(\theta)}$, and the QNE are the eigenvectors corresponding to eigenvalues Λ. To compute the QNMs and QNEs then, we first search for the zeros to the function

$$F(\omega) \equiv \left| \Lambda_{(\rho)}(\omega) - \Lambda_{(\theta)}(\omega) \right|. \tag{39}$$

We choose $\Lambda_{(\rho)}$ to be the smallest (in absolute magnitude) eigenvalue from the radial system, and choose $\Lambda_{(\theta)}$ to be the lth smallest (in absolute value) eigenvalue from the angular equation. We search for the zeros of F using Newton's method

$$\omega_{(n+1)} = \omega_{(n)} - \gamma \frac{F}{F'} \Big|_{\omega = \omega_{(n)}}, \tag{40}$$

where $0 < \gamma \leq 1$, and F' denotes the complex derivative of F, which we compute using a second-order accurate finite difference stencil (here $0 < \epsilon \ll 1$ is a real number):

$$F'\big|_{\omega = \omega_{(n)}} \approx \frac{F\left(\omega_{(n)} + \epsilon\right) - F\left(\omega_{(n)} - \epsilon\right)}{2\epsilon} + \frac{F\left(\omega_{(n)} + i\epsilon\right) + F\left(\omega_{(n)} - i\epsilon\right)}{2i\epsilon}. \tag{41}$$

In our search for QNMs, we can exclude modes with positive imaginary part as there are no such mode solutions for the Teukolsky equation, even in the extremal limit [36, 37].

The angular separation constants Λ and QNMs ω have an unambiguous labeling in azimuthal angular number m and black hole spin a/M, but there is some ambiguity in their labeling (n, l); for more discussion see [34].

¶ We note that this method has been used to compute the QNMs and QNEs for spherically symmetric black hole spacetimes [33].

5. Results: quasinormal modes and quasinormal eigenfunctions

We next present several example QNEs which we computed using a code that implements the algorithm described in Sec. 4 [24]. In the plots we show, we began with "seed" values for (ω, Λ) computed from the `qnm` package for that mode, and then let the root-finding algorithm in our code relax to the final (ω, Λ). We find the resulting (ω, Λ) to be identical (to within numerical precision) to the value given by the `qnm` code (see Table. 1). We normalize the radial eigenfunctions so that their maximum amplitude is equal to one.

5.1. Moderate black hole spin quasinormal mode eigenfunctions

In Fig. 2 we plot the QNEs for the $s = -2, n = 0, l = 2, m = 2$ QNMs, for small to moderately large black hole spins. In the upper two panels we present the real and imaginary parts of the radial part of the QNE. In the lower left panel we plot the absolute value of the Chebyshev coefficients for the radial part of the QNE. Finally, in the lower right panel we plot the absolute value of the spin-weighted spherical harmonic coefficients for the QNE. For slowly/moderately spinning black holes, we see that with around 20 Chebyshev and spin-weighted spherical harmonics we can describe the eigenfunctions for the fundamental $s = -2, l = 2, m = 2$ mode to high precision. We show a similar set of figures for the $s = -1, n = 0, l = 1, m = 1$ quasinormal modes in Fig. 3.

5.2. Near-extremal quasinormal mode solutions

There exists a family of QNMs whose imaginary part tends to zero in the extremal black hole spin limit $(a/M \to 1)$. In [40, 41] these modes were called *zero-damped* QNMs, as the imaginary part of a QNM determines its characteristic damping time (see also [38, 39]). These modes exist for all $l, m \geq 0$, and the mode frequency takes the form

$$M\omega \approx \frac{m}{2} - \Omega_\epsilon \left(\frac{\epsilon}{2}\right)^{1/2} + \mathcal{O}(\epsilon), \tag{42}$$

where we have defined

$$\Omega_\epsilon \equiv \left(\frac{7}{4}m^2 - \left(s + \frac{1}{2}\right)^2 - {}_s\Lambda_l^m\right)^{1/2} + i\left(n + \frac{1}{2}\right), \tag{43}$$

$$\epsilon \equiv 1 - \frac{a}{M}. \tag{44}$$

In near-extremal limit, we observe that the QNEs associated with the zero-damped QNMs (at least for spin-weights $s = -2, -1$) become sharply peaked near the black hole horizon; see Fig. 4 and Fig. 5. We find that stably solving for the radial part of the QNE for spins very near extremality requires the use the use of higher-precision arithematic. We present the largest spin $(a = 0.99999)$ QNMs and QNEs that we can resolve with 244 radial Chebyshev coefficients and 1024 bits of floating-point precision. As noted by Cook and Zalutskiy [34], we do not need increasingly more spin-weighted spherical harmonics to resolve the angular part of the QNE as we approach the extremal black hole limit. We show three more examples near-extremal $s = -2$ QNEs in Fig. 6.
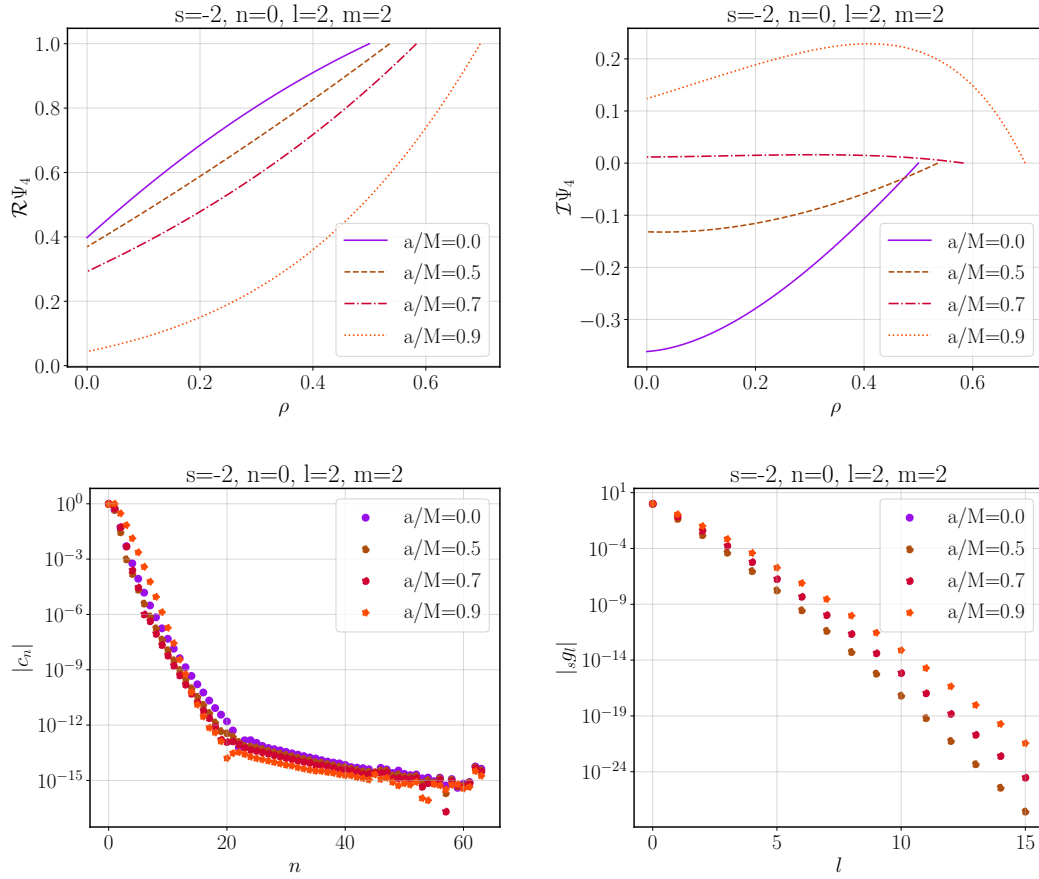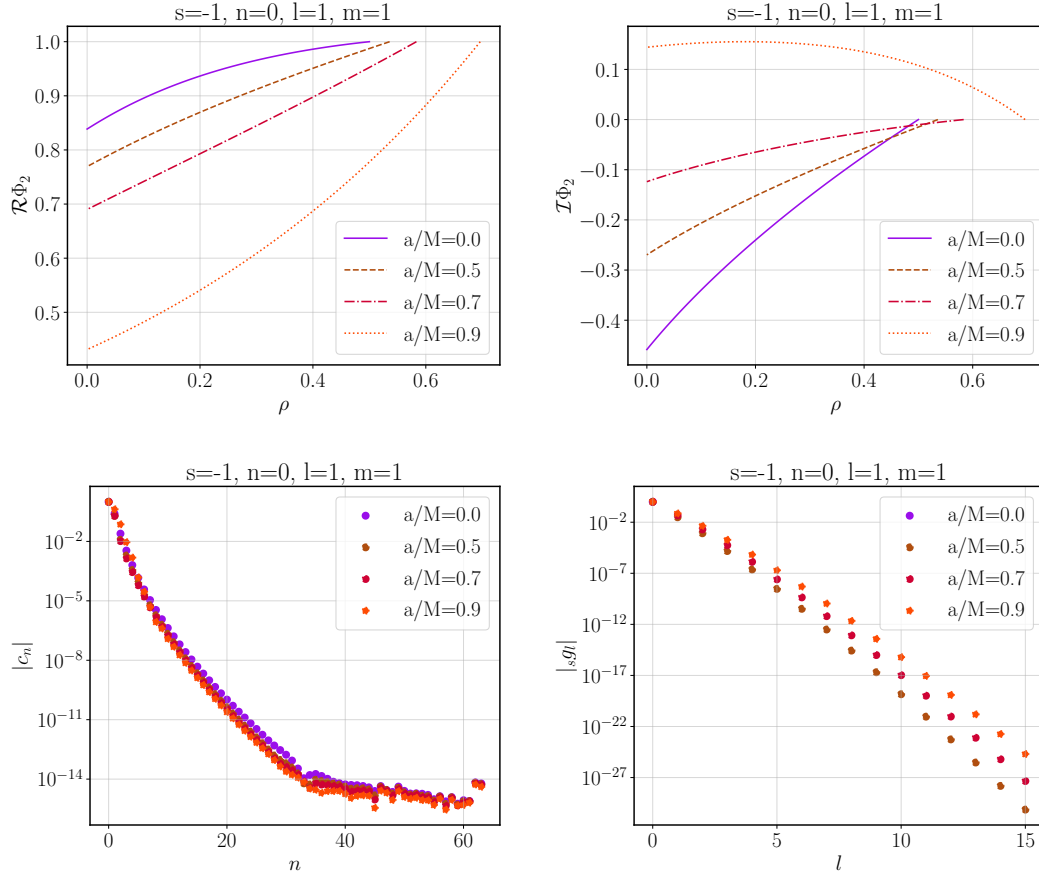
Figure 2. The $s = -2$ QNEs for relatively low spins. Future null infinity is located at $\rho = 0$, and the black hole horizon is located at $\rho = \rho_+$, which changes with the black hole spin. The lower left panel plots the absolute value of the Chebyshev coefficients, $|c_n|$, used to fit the radial mode, and the lower right panel shows the absolute value of the spin-weighted spherical harmonic coefficients for the QNE.

From those figures, we see that the $n = 0, l = 2, m = 0, -2$ QNEs appear to remain smooth in the extremal limit, while the radial derivative of the $n = 0, l = m = 3$ QNEs appear to blow up in that limit. We note that the $n = 0, l = 2, m = 0, -2$ QNMs are not zero-damped, while the $n = 0, l = m = 3$ QNMs are; see Table 1 or [40] for more discussion.

We provide a semi-analytic argument to explain growth in the radial gradient of the zero-damped QNE grow near the black hole horizon as $\epsilon \to 0$. The derivative of the near-horizon solution (Eq. 36), to leading order in $x \ll 1$ is:

$$\frac{dR_{\mathcal{H}}}{d\rho} = \mathcal{A}_{\mathcal{H}} \frac{1}{\rho_+} \left(\frac{a_{\mathcal{H}} b_{\mathcal{H}}}{c_{\mathcal{H}}} + \mathcal{O}\left(x\right) \right). \tag{45}$$

We next expand in the near-extremal limit (i.e. in ϵ), and plug in the zero-damped value for the QNM (Eq. 42). This formula fits our numerical data for the zero-damped modes well when $\epsilon \ll 1$; see Table 1. Plugging into Eq. 45 the above value for ω, along

Figure 3. The $s = -1$ QNEs for relatively low spins. Future null infinity is located at $\rho = 0$, and the black hole horizon is located at $\rho = \rho_+$, which changes with the black hole spin. The lower left panel plots the absolute value of the Chebyshev coefficients, $|c_n|$, used to fit the radial mode, and the lower right panel shows the absolute value of the spin-weighted spherical harmonic coefficients for the QNE.

with using Eqns. 31, 33, and

$$a/M = 1 + \epsilon, \qquad M\rho_+ = 1 - (2\epsilon)^{1/2} + \mathcal{O}(\epsilon), \tag{46}$$

we find that

$$\frac{dR_\mathcal{H}}{d\rho} = \frac{\mathcal{A}_\mathcal{H} M}{2\sqrt{2}} \times \left(\frac{\frac{3}{4}m^2 - 2s + im(2s - 1) + {}_s\Lambda_l^m}{1 - s - im + i\Omega_\epsilon} \frac{1}{\sqrt{\epsilon}} + \mathcal{O}(1) \right). \tag{47}$$

We see that as $\epsilon \to 0$ that the derivative of the near-horizon ($x \ll 1$) solution blows up when we plug in the zero-damped mode ansatz. This calculation agrees qualitatively with what we see in our numerical computations of the zero-damped QNEs; (see Figs. 4, 5, 6).

In the coordinates we are using, the radial proper distance does not blow up near the black hole horizon; see Eq. 13. Because of this, we can conclude that $\frac{dR_\mathcal{H}}{dr} = -\frac{1}{r^2} \frac{dR_\mathcal{H}}{d\rho}$, also grows larger in the limit $a/M \to 1$ near the black hole horizon for the zero-damped QNMs.
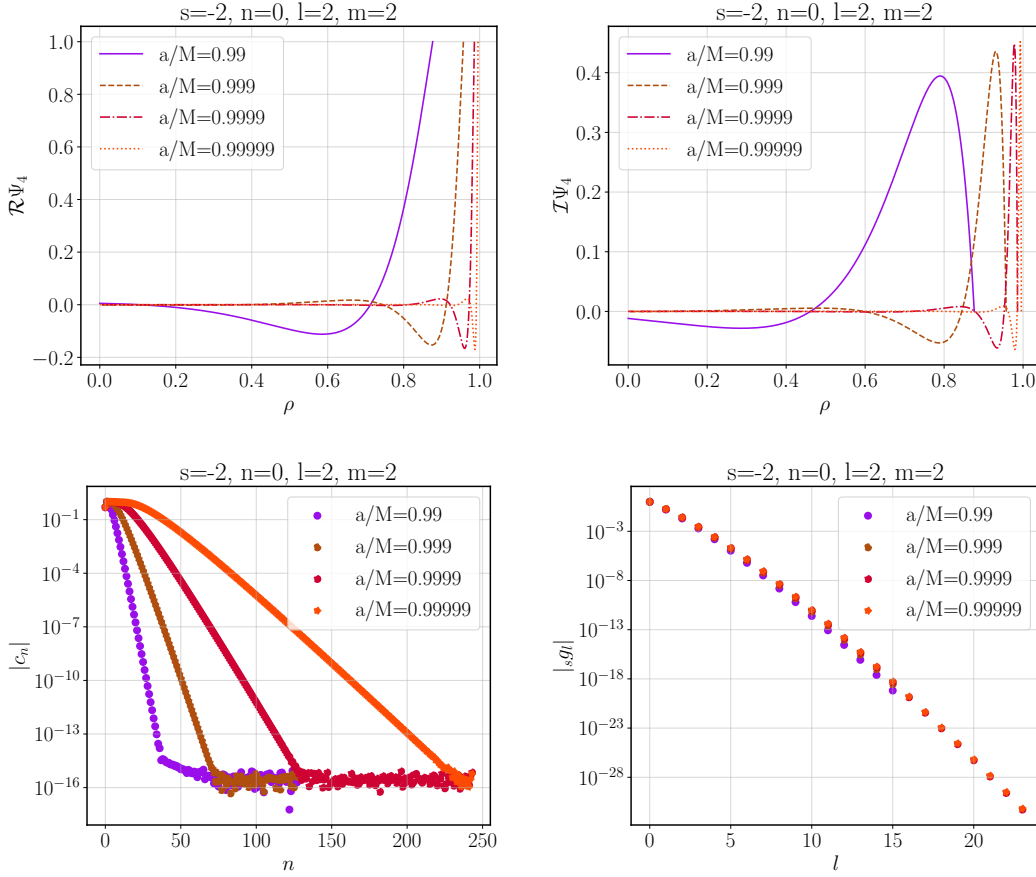
Figure 4. The $s = -2$ QNEs in the limit of relatively high black hole spins. Future null infinity is located at $\rho = 0$, and the black hole horizon is located at $\rho = \rho_+$, which changes with the black hole spin. As we increase the black hole spin, we need to increase the resolution in the radial direction, but not significantly in the angular direction. We see that as $a \to 1$, the QNEs become localized near the black hole horizon.

6. Discussion

We have computed several of the quasinormal modes and their associated quasinormal eigenfunctions of the Teukolsky equation. These calculations were performed in horizon-penetrating, hyperboloidally-compactified (HPHC) coordinates. With these coordinates (and with a suitable choice of tetrad), the QNEs of the Teukolsky equation are regular, including at the black hole horizon and future null infinity. In the process of computing the QNMs and QNEs, we have found that the eigenfunctions for the zero-damped modes develop a steep radial gradient near the black hole horizon in the near-extremal Kerr limit ($a/M \to 1$). This feature of the mode solutions makes resolving the zero-damped QNEs increasingly difficult as the black hole spin approaches extremality.

For future work, it would be interesting to further investigate the properties of QNE solutions, such as the properties of the solutions in the limit of large overtone number.
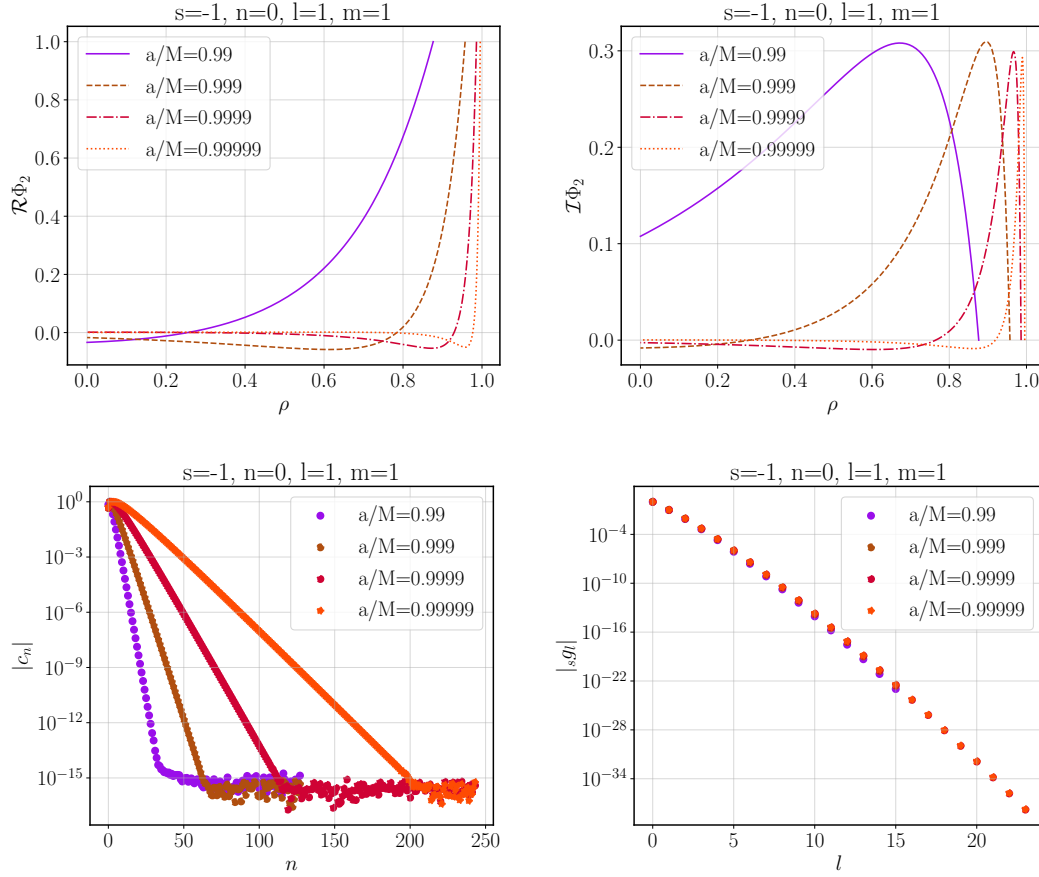
Figure 5. The $s = -1$ QNEs in the limit of relatively high black hole spins. Future null infinity is located at $\rho = 0$, and the black hole horizon is located at $\rho = \rho_+$, which changes with the black hole spin. As we increase the black hole spin, we need to increase the resolution in the radial direction, but not significantly in the angular direction. We see that as $a \to 1$, the QNEs become localized near the black hole horizon.

The properties of the QNE solutions in the near-extremal Kerr limit also deserve further study, given the variety QNM solutions that can be found in that limit [38, 39, 40, 42, 41]. Aretakis has shown that extremal Kerr black hole spacetimes are unstable at the black hole horizon [43, 44]. This instability arises from outgoing wave solutions that have support at the black hole horizon, which develop gradients in the radial direction that grow unbounded over time. Similar results have been found for the zero-damped QNM solutions of the near-extremal Kerr spacetime [45, 46]. It would be interesting to connect the results of our study to previous work on the Aretakis instability (for example, one may expect that given Aretakis' result, zero-damped QNE solutions in the extremal limit become step-function like). As we mentioned in the Introduction, it would be interesting to apply our results to a computation of the pseudospectrum of quasinormal modes of the Teukolsky equation, thus extending the work of [17, 18] to that spacetime. Finally, another direction for potential work would be to extend this work to computing
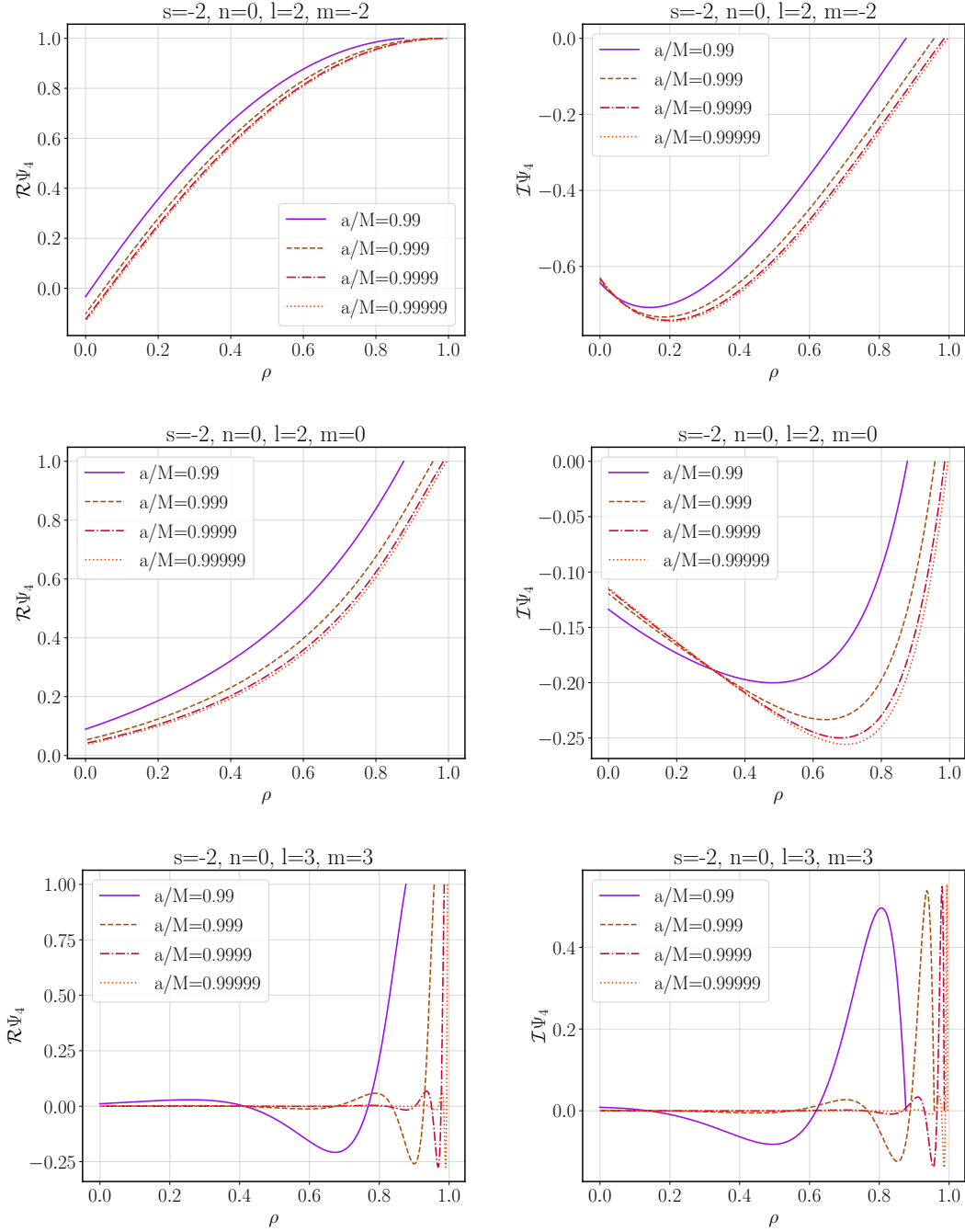
Figure 6. Other example $s = -2$ quasinormal mode radial eigenfunctions in the near-extremal limit. Here we only plot the real and imaginary parts of Ψ_4, and do not plot the Chebyshev or angular coefficients. We see that the $l = 2, m = 0, -2$ QNEs remain smooth as $a/M \to 1$, which the radial derivative of the $n = 0, l = m = 3$ QNEs appear to blow up in the limit $a/M \to 1$. The $l = 2, m = 0, -2$ modes we consider are not zero-damped in the extremal limit, while the $l = m = 3$ mode we consider is (see Table. 1); for more discussion of zero-damped modes see [38, 39, 40, 41].

the QNEs to the Kerr-Newman spacetime in HPHC coordinates [47].

The numerical methodology we use to compute the QNEs could be improved as well. While the pseudospectral Chebyshev approach we use to compute the radial QNEs naturally impose regular boundary conditions on the solution, we have found that we had to use many ($N_{(\rho)} > 200$) Chebyshev coefficients to properly resolve the zero-damped QNEs in the near-extremal limit. We have also found that significantly more Chebyshev coefficients are needed to resolve higher overtones, regardless of the value of the black hole spin. As Chebyshev derivative matrices are very poorly conditioned, this then requires the use of higher-precision arithematic, which dramatically slows down the speed at which we can compute quasinormal mode solutions. A modification of Leaver's method (that is, a spectral expansion in a series of rational polynomials of ρ) may provide a more reliable and stable method to obtain quasinormal modes in HPHC coordinates.

Acknowledgments

Appendix .1. Quasinormal modes and convergence

In Table. 1 we list QNMs as computed using the code [24]. These QNMs agree with those computed from the `qnm` code [23] to the precision given in the table (except for the $s = -2, n = 0, l = m = -2$ mode; see the caption to the Table).

(s,n,l,m)	a	$M\omega$	${}_s\Lambda_l^m$
$(-2, 0, 2, 2)$	0	$0.3736716 - 0.0889623i$	4
$(-2, 0, 2, 2)$	0.5	$0.4641230 - 0.0856388i$	$3.3423 + 0.1292i$
$(-2, 0, 2, 2)$	0.7	$0.5326002 - 0.0807928i$	$2.9032 + 0.1832i$
$(-2, 0, 2, 2)$	0.9	$0.6716142 - 0.0648692i$	$2.1098 + 0.2111i$
$(-2, 0, 2, 2)$	0.99	$0.8708926 - 0.0293904i$	$1.1196 + 0.1180i$
$(-2, 0, 2, 2)$	0.999	$0.9558544 - 0.0105305i$	$0.7357 + 0.0443i$
$(-2, 0, 2, 2)$	0.9999	$0.9856735 - 0.0034686i$	$0.6055 + 0.0148i$
$(-2, 0, 2, 2)$	0.99999	$0.9954317 - 0.0011112i$	$0.5633 + 0.0047i$
$(-2, 0, 2, -2)$	0.99	$0.2921067 - 0.0880523i$	$4.7163 - 0.1966i$
$(-2, 0, 2, -2)$	0.999	$0.2916086 - 0.0880285i$	$4.7212 - 0.1981i$
$(-2, 0, 2, -2)$	0.9999	$0.2915590 - 0.0880261i$	$4.7217 - 0.1983i$
$(-2, 0, 2, -2)$	0.99999	$0.2915567 - 0.0880160i$	$4.7218 - 0.1981i$
$(-2, 0, 2, 0)$	0.99	$0.4236846 - 0.0727008i$	$3.9102 + 0.0319i$
$(-2, 0, 2, 0)$	0.999	$0.4249978 - 0.0718986i$	$3.9079 + 0.0322i$
$(-2, 0, 2, 0)$	0.9999	$0.4251304 - 0.0718155i$	$3.9077 + 0.0323i$
$(-2, 0, 2, 0)$	0.99999	$0.4251435 - 0.0718072i$	$3.9076 + 0.0323i$
$(-2, 0, 3, 3)$	0.99	$1.3230831 - 0.029403i$	$6.4040 + 0.1043i$
$(-2, 0, 3, 3)$	0.999	$1.4397481 - 0.010530i$	$5.9312 + 0.0397i$
$(-2, 0, 3, 3)$	0.9999	$1.4804730 - 0.003469i$	$5.7714 + 0.0133i$
$(-2, 0, 3, 3)$	0.99999	$1.4937761 - 0.001111i$	$5.7197 + 0.0043i$
$(-1, 0, 1, 1)$	0.0	$0.2482633 - 0.092488i$	2
$(-1, 0, 1, 1)$	0.5	$0.2940910 - 0.087677i$	$1.8419 + 0.0511i$
$(-1, 0, 1, 1)$	0.7	$0.3266554 - 0.081869i$	$1.7436 + 0.0724i$
$(-1, 0, 1, 1)$	0.9	$0.3875811 - 0.065625i$	$1.5832 + 0.0835i$
$(-1, 0, 1, 1)$	0.99	$0.4633988 - 0.031292i$	$1.4185 + 0.0482i$
$(-1, 0, 1, 1)$	0.999	$0.4896711 - 0.011609i$	$1.3700 + 0.0185i$
$(-1, 0, 1, 1)$	0.9999	$0.4971357 - 0.003805i$	$1.3573 + 0.0061i$
$(-1, 0, 1, 1)$	0.99999	$0.4991753 - 0.001177i$	$1.3539 + 0.0019i$

Table 1. Computed QNMs and separation constants, computed using the code [24], which implements the algorithm in Sec. 4. To produce accurate results at high spin using the radial pseudospectral method, we had to resort to using higher-precision arithematic (here: 1024 bits of precision). These results agree with those computed from the `qnm` code [23] to the precision presented, except for the $s = -2, n = 0, l = 2, m = -2$ mode, where there is a difference between the qnm code in the last two decimal places for the values of ω and ${}_s\Lambda_l^m$.

We next present an example convergence test of a QNE in Fig. 1. We see that the pointwise difference between a "low" and "medium" resolution calculations is larger than the difference between a "medium" and "high" resolution calculation. These calculations were performed with 1024 bit precision, and the resolutions of the low, med, high resolution calculations were respectively $(N_{(\rho)} = 204, N_{(\theta)} = 20)$,

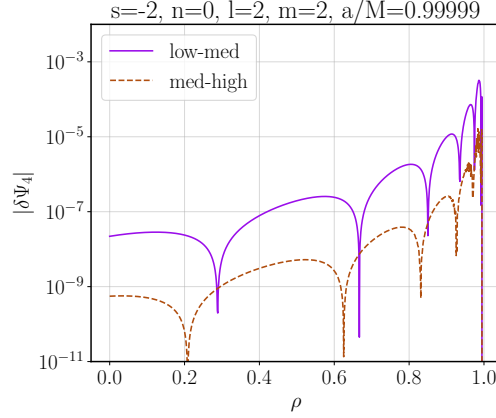$(N_{(\rho)} = 224, N_{(\theta)} = 22)$, and $(N_{(\rho)} = 244, N_{(\theta)} = 24)$.

Figure 1. Convergence study of the radial part of the $s = -2, n = 0, l = 2, m = 2$ QNE for a black hole spin parameter $a/M = 0.99999$. These calculations were performed with 1024 bit precision, and the resolutions of the low, med, high resolution calculations were respectively $(N_{(\rho)} = 204, N_{(\theta)} = 20)$, $(N_{(\rho)} = 224, N_{(\theta)} = 22)$, and $(N_{(\rho)} = 244, N_{(\theta)} = 24)$.

Appendix A. Some properties of the Jacobi polynomials and spin-weighted spherical harmonics

Appendix A.1. Jacobi polynomials

Our notation follows [29] (see also, e.g. [30] for a more general reference). The Jacobi polynomials are orthogonal with respect to the weight $w = (1 - x)^\alpha (1 + x)^\beta$ on the interval $(-1, 1)$. They are denoted by:

$$P_n^{(\alpha,\beta)}(x), \qquad n = 0, 1, 2, ... \alpha, \beta > -1 \tag{A.1}$$

The Jacobi polynomials satisfy the following orthogonality condition

$$\int_{-1}^{1} dx \, (1 - x)^\alpha (1 + x)^\beta \, P_n^{(\alpha,\beta)}(x) P_m^{(\alpha,\beta)}(x) =$$

$$\frac{2^{\alpha+\beta+1}}{2n + \alpha + \beta + 1} \frac{\Gamma(n + \alpha + 1) \Gamma(n + \beta + 1)}{n! \Gamma(n + \alpha + \beta + 1)} \delta_{nm}. \tag{A.2}$$

The derivative and recursion relations for the Jacobi polynomials are

$$\frac{d}{dx} P_n^{(\alpha,\beta)}(x) = \frac{1}{2}(n + \alpha + \beta + 1) P_{n-1}^{(\alpha+1,\beta+1)}(x), \tag{A.3}$$

$$\frac{(2n+2)(n+\alpha+\beta+1)}{2n+\alpha+\beta+1} P_{n+1}^{(\alpha,\beta)}(x) = \left[\frac{\alpha^2 - \beta^2}{2n+\alpha+\beta} + (2n+\alpha+\beta+2)\,x \right] P_n^{(\alpha,\beta)}(x)$$

$$- \frac{2(2n+\alpha+\beta+2)(n+\alpha)(n+\beta)}{(2n+\alpha+\beta)(2n+\alpha+\beta+1)} P_{n-1}^{(\alpha,\beta)}(x). \tag{A.4}$$

Appendix A.2. Spin-weighted spherical harmonics

We work in spherical polar coordinates. The spin-weighted spherical harmonics are a complete set of orthogonal functions on the sphere for spin-weighted functions. They are eigenfunctions for the spin-weighted spherical Laplacian:

$$\frac{1}{\sin\theta}\partial_\theta\left(\sin\theta\partial_\theta {}_sY_l^m(\theta,\phi)\right)$$

$$+ \left(s - \frac{(-i\partial_\phi + s\cos\theta)^2}{\sin^2\theta} + (l-s)(l+s+1)\right) {}_sY_l^m(\theta,\phi) = 0. \tag{A.5}$$

The spin-weighted spherical harmonics can be written as

$$ {}_sY_l^m(\theta,\phi) = e^{im\phi}\, {}_sP_l^m(\theta), \tag{A.6}$$

where ${}_sP_l^m(y)$ is the spin-weighted associated Legendre polynomial. These functions are related to the Jacobi polynomials via (e.g. [48, 16]):

$$ {}_sP_l^m(y) = {}_s\mathcal{N}_l^m (1-y)^\alpha (1+y)^\beta P_n^{(\alpha,\beta)}(y), \tag{A.7}$$

where $y \equiv -\cos\theta$, $\alpha \equiv |m-s|$, $\beta \equiv |m+s|$, $n \equiv l - \frac{\alpha+\beta}{2}$, and

$$ {}_s\mathcal{N}_l^m \equiv (-1)^{\max(m,-s)} \left(\frac{2n+\alpha+\beta+1}{2^{\alpha+\beta+1}}\frac{n!\,(n+\alpha+\beta)!}{(n+\alpha)!\,(n+\beta)!}\right)^{1/2}. \tag{A.8}$$

From the recursion relation for the Jacobi polynomials, Eq. A.4, and the normalization of the spin-weighted spherical harmonics, Eq. A.8, we have [49, 34]

$$y\, {}_sP_l^m(y) = {}_s\mathcal{A}_l^m\, {}_sP_{l+1}^m(y) + {}_s\mathcal{B}_l^m\, {}_sP_l^m(y) + {}_s\mathcal{C}_l^m\, {}_sP_{l-1}^m(y), \tag{A.9}$$

where

$$ {}_s\mathcal{A}_l^m = \frac{2}{(2n+\alpha+\beta+2)}\left[\frac{(n+1)(n+\alpha+1)(n+\beta+1)(n+\alpha+\beta+1)}{(2n+\alpha+\beta+1)(2n+\alpha+\beta+3)}\right]^{1/2}$$

$$= \left[\frac{((l+1)^2-s^2)((l+1)^2-m^2)}{(l+1)^2(2l+1)(2l+3)}\right]^{1/2}, \tag{A.10}$$

$$ {}_s\mathcal{B}_l^m = -\frac{\alpha^2-\beta^2}{(2n+\alpha+\beta)(2n+\alpha+\beta+2)}$$

$$= -\frac{ms}{l(l+1)}, \tag{A.11}$$

$$ {}_s\mathcal{C}_l^m = \frac{2}{(2n+\alpha+\beta)}\left[\frac{n(n+\alpha)(n+\beta)(n+\alpha+\beta)}{(2n+\alpha+\beta+1)(2n+\alpha+\beta-1)}\right]^{1/2}$$

$$= \left[\frac{(l^2-s^2)(l^2-m^2)}{l^2(4l^2-1)}\right]^{1/2}. \tag{A.12}$$

Appendix B. Converting angular ODE to a sparse matrix equation in spectral space

For completeness we review a spectral method that converts the angular equation, Eq. 17, into a sparse linear-algebra problem[34, 35]. We recall that Eq. 17 is solved

by the spin-weighted spheroidal harmonics

$$S = {}_sS_l^m(\theta, c).$$ (B.1)

When $a = 0$ the equation reduces to that of the spin-weighted spherical harmonics. We expand the spin-weighted spheroidal harmonics in terms of spin-weighted spherical harmonics (which form a basis for spin-weighted functions on the sphere):

$${}_sS_l^m(\theta, \phi, c) = \sum_{l'} {}_sg_{l,l'}^m(a\omega)\, {}_sY_{l'}^m(\theta, \phi) = \sum_{l'} {}_sg_{l,l'}^m(a\omega)\, {}_sP_{l'}^m(\theta)\, e^{im\phi}, \quad \text{(B.2)}$$

where ${}_sP_{l'}^m$ are the spin-weighted associated Legendre polynomials. This approach was first used in the context of numerically computing QNM in [34] (although similar earlier semi-analytic works include [50, 49]). We expand S in terms of spherical harmonics, and use Eq. A.5 to rewrite Eq. 17 as

$$\frac{1}{\sin\theta}\frac{d}{d\theta}\left(\sin\theta\frac{d\,{}_sS_l^m}{d\theta}\right) + \left(s - \frac{(m + s\cos\theta)^2}{\sin^2\theta} - 2a\omega s\cos\theta + a^2\omega^2\cos^2\theta + {}_s\Lambda_l^m\right){}_sS_l^m$$

$$= e^{im\phi}\sum_{l'}\left(-2a\omega s\cos\theta + a^2\omega^2\cos^2\theta - (l' - s)(l' + s + 1) + {}_s\Lambda_l^m\right){}_sg_{l,l'}^m{}_sP_{l'}^m(\theta) = 0$$

$$= e^{im\phi}\left({}_s\vec{g}_l^m, \left[-\hat{M}_{(\theta)}^T + {}_s\Lambda^m\hat{I}\right]{}_s\vec{P}^m\right), \quad \text{(B.3)}$$

where

$$\left[\hat{M}_\theta^T\right]_{l,l'} \equiv (a\omega)^2\left[\hat{Y}_1^2\right]_{l,l'} - 2s(a\omega)\left[\hat{Y}_1\right]_{l,l'} - \delta_{l,l'}(l' - s)(l' + s + 1). \quad \text{(B.4)}$$

Here we have defined the matrix (see Eq. A.9)

$$y_s\vec{P}^m \equiv \hat{Y}_1{}_s\vec{P}^m. \quad \text{(B.5)}$$

For a fixed (s, m, a), we then have the sparse matrix eigenvalue equation

$$\left(\hat{M}_{(\theta)} - \Lambda\hat{I}\right)\vec{g} = 0. \quad \text{(B.6)}$$

Appendix C. Chebyshev pseudospectral discretization of the radial ODE

We briefly review Chebyshev (pseudospectral) collocation methods [31, 32]. See also [33, 17] for other recent examples of applying pseudospectral methods to calculating the QNMs and QNEs of the various wave equations for spherically symmetric black hole spacetimes.

The Chebyshev polynomials (of the first kind) of order n are given by

$$T_n(x) = \cos(n\arccos x), \qquad x \in [-1, 1]. \quad \text{(C.1)}$$

The Chebyshev polynomials form an orthonormal basis for functions $f \in L^2([-1, 1], w(x)dx)$, where $w(x) = (1 - x^2)^{-1/2}$, in particular they satisfy

$$\int_{-1}^1 \frac{dx}{\sqrt{1 - x^2}}T_n(x)T_m(x) = \begin{cases} 0 & n \neq m \\ \frac{\pi}{2} & n = m \neq 0, \\ \pi & n = m = 0 \end{cases} \quad \text{(C.2)}$$

One can expand essentially any sufficiently smooth function on the interval $[-1, 1]$ as a sum of Chebyshev polynomials

$$f(x) = \frac{1}{2}c_0 + \sum_{n=1}^{\infty} c_n T_n(x). \tag{C.3}$$

We discretize the radial ODE using the Chebyshev extreme points as the collocation points. On the interval $[-1, 1]$, they are

$$x_j = \cos\left(\frac{\pi j}{N}\right), \qquad j = 0, 1, ..., N, \tag{C.4}$$

which we map to the interval $[0, \rho_+]$ via $\rho_j = \rho_+ (x_j + 1)/2$. With this method, the derivative operators are converted into dense matrices, whose components take the form

$$D_{ij} = \frac{dT_i}{dx}\Big|_{x=x_j}. \tag{C.5}$$

Explicitly we have

$$D_{ij} = \begin{cases} -\frac{2N^2+1}{6} & i = j = N \\ \frac{2N^2+1}{6} & i = j = 0 \\ -\frac{x_j}{2(1-x_j^2)} & 0 < i = j < N \\ \frac{c_i}{c_j} \frac{(-1)^{i+j}}{(x_i - x_j)} & i \neq j, \qquad i, j = 1, ..., N-1 \end{cases}, \tag{C.6}$$

where $c_0 = c_N = 2$ and $c_1 = \cdots = c_{N-1} = 1$. We can define a second derivative matrix using

$$D_{ij}^{(2)} = \sum_k D_{ik} D_{kj}. \tag{C.7}$$

These derivative matrices are generally ill-conditioned (the condition number for $D_{ij}^{(2)}$ goes as N^4, where N is the size of the matrix [31, 32]), but we have empirically found that the `eigen` function in the `Julia` standard library [51], (sometimes augmented with higher precision arithematic using the `GenericSchur` library [52]–with floating point numbers the `eigen` library simply calls a LAPACK routine [53]) that we can stably obtain the eigenvalues and eigenvectors to the radial ODE, even with matrices larger than 100×100.

[1] Zenginoglu A 2011 *Phys. Rev. D* **83** 127502 (*Preprint* `1102.2451`)
[2] Teukolsky S A 1973 *Astrophys. J.* **185** 635–647
[3] Nollert H P 1999 *Class. Quant. Grav.* **16** R159–R216
[4] Kokkotas K D and Schmidt B G 1999 *Living Rev. Rel.* **2** 2 (*Preprint* `gr-qc/9909058`)
[5] Berti E, Cardoso V and Starinets A O 2009 *Class. Quant. Grav.* **26** 163001 (*Preprint* `0905.2975`)
[6] Konoplya R A and Zhidenko A 2011 *Rev. Mod. Phys.* **83** 793–836 (*Preprint* `1102.4014`)
[7] Boyer R H and Lindquist R W 1967 *Journal of Mathematical Physics* **8** 265–281 (*Preprint* `https://doi.org/10.1063/1.1705193`) URL `https://doi.org/10.1063/1.1705193`
[8] Regge T and Wheeler J A 1957 *Phys. Rev.* **108**(4) 1063–1069 URL `https://link.aps.org/doi/10.1103/PhysRev.108.1063`
[9] Zerilli F J 1970 *Phys. Rev. Lett.* **24**(13) 737–738 URL `https://link.aps.org/doi/10.1103/PhysRevLett.24.737`
[10] Bardeen J M and Press W H 1973 *Journal of Mathematical Physics* **14** 7–19 (*Preprint* `https://doi.org/10.1063/1.1666175`) URL `https://doi.org/10.1063/1.1666175`
[11] Leaver E W 1985 *Proc. Roy. Soc. Lond. A* **402** 285–298

[12] Teukolsky S A and Press W H 1974 *Astrophys. J.* **193** 443–461
[13] Zenginoglu A and Khanna G 2011 *Phys. Rev. X* **1** 021017 (*Preprint* 1108.1816)
[14] Harms E, Bernuzzi S and Brügmann B 2013 *Class. Quant. Grav.* **30** 115013 (*Preprint* 1301.1591)
[15] Csukás K, Rácz I and Tóth G Z 2019 *Phys. Rev. D* **100** 104025 (*Preprint* 1905.09082)
[16] Ripley J L, Loutrel N, Giorgi E and Pretorius F 2021 *Phys. Rev. D* **103** 104018 (*Preprint* 2010.00162)
[17] Jaramillo J L, Panosso Macedo R and Al Sheikh L 2021 *Phys. Rev. X* **11** 031003 (*Preprint* 2004.06434)
[18] Destounis K, Macedo R P, Berti E, Cardoso V and Jaramillo J L 2021 *Phys. Rev. D* **104** 084091 (*Preprint* 2107.09673)
[19] Trefethen L, Embree M and Embree M 2005 *Spectra and Pseudospectra: The Behavior of Nonnormal Matrices and Operators* (Princeton University Press) ISBN 9780691119465 URL https://books.google.co.uk/books?id=7gIbT-Y7-AIC
[20] Loutrel N, Ripley J L, Giorgi E and Pretorius F 2021 *Phys. Rev. D* **103** 104017 (*Preprint* 2008.11770)
[21] Cheung M H Y, Destounis K, Macedo R P, Berti E and Cardoso V 2021 (*Preprint* 2111.05415)
[22] Sberna L, Bosch P, East W E, Green S R and Lehner L 2021 (*Preprint* 2112.11168)
[23] Stein L C 2019 *J. Open Source Softw.* **4** 1683 (*Preprint* 1908.10377)
[24] Ripley J L 2022 TeukolskyQNMFunctions.jl URL https://github.com/JLRipley314/TeukolskyQNMFunctions.jl
[25] Zenginoglu A 2008 *Class. Quant. Grav.* **25** 145002 (*Preprint* 0712.4333)
[26] Panosso Macedo R 2020 *Class. Quant. Grav.* **37** 065019 (*Preprint* 1910.13452)
[27] Sasaki M and Nakamura T 1982 *Physics Letters A* **89** 68–70 ISSN 0375-9601 URL https://www.sciencedirect.com/science/article/pii/0375960182905072
[28] Hughes S A 2000 *Phys. Rev. D* **62** 044029 [Erratum: Phys.Rev.D 67, 089902 (2003)] (*Preprint* gr-qc/0002043)
[29] Beals R and Wong R 2016 *Special Functions and Orthogonal Polynomials* Cambridge Studies in Advanced Mathematics (Cambridge University Press) ISBN 9781107106987 URL https://books.google.co.uk/books?id=RusIDAAAQBAJ
[30] *NIST Digital Library of Mathematical Functions* http://dlmf.nist.gov/, Release 1.1.2 of 2021-06-15 f. W. J. Olver, A. B. Olde Daalhuis, D. W. Lozier, B. I. Schneider, R. F. Boisvert, C. W. Clark, B. R. Miller, B. V. Saunders, H. S. Cohl, and M. A. McClain, eds. URL http://dlmf.nist.gov/
[31] Trefethen L 2000 *Spectral Methods in MATLAB* Software, Environments, and Tools (Society for Industrial and Applied Mathematics) ISBN 9780898714654 URL https://books.google.co.uk/books?id=cosg8VUwVI4C
[32] Boyd J 2001 *Chebyshev and Fourier Spectral Methods: Second Revised Edition* Dover Books on Mathematics (Dover Publications) ISBN 9780486411835 URL https://books.google.co.uk/books?id=i9UoAwAAQBAJ
[33] Jansen A 2017 *Eur. Phys. J. Plus* **132** 546 (*Preprint* 1709.09178)
[34] Cook G B and Zalutskiy M 2014 *Phys. Rev. D* **90** 124021 (*Preprint* 1410.7698)
[35] Hughes S A 2000 *Phys. Rev. D* **61** 084004 [Erratum: Phys.Rev.D 63, 049902 (2001), Erratum: Phys.Rev.D 65, 069902 (2002), Erratum: Phys.Rev.D 67, 089901 (2003), Erratum: Phys.Rev.D 78, 109902 (2008), Erratum: Phys.Rev.D 90, 109904 (2014)] (*Preprint* gr-qc/9910091)
[36] Whiting B F 1989 *J. Math. Phys.* **30** 1301
[37] Teixeira da Costa R 2020 *Commun. Math. Phys.* **378** 705–781 (*Preprint* 1910.02854)
[38] Hod S 2008 *Phys. Rev. D* **78** 084035 (*Preprint* 0811.3806)
[39] Hod S 2009 *Phys. Rev. D* **80** 064004 (*Preprint* 0909.0314)
[40] Yang H, Zhang F, Zimmerman A, Nichols D A, Berti E and Chen Y 2013 *Phys. Rev. D* **87** 041502 (*Preprint* 1212.3271)
[41] Yang H, Zimmerman A, Zenginoğlu A, Zhang F, Berti E and Chen Y 2013 *Phys. Rev. D* **88** 044047 (*Preprint* 1307.8086)

[42] Yang H, Nichols D A, Zhang F, Zimmerman A, Zhang Z and Chen Y 2012 *Phys. Rev. D* **86** 104006 (*Preprint* `1207.4253`)

[43] Aretakis S 2012 *J. Funct. Anal.* **263** 2770–2831 (*Preprint* `1110.2006`)

[44] Aretakis S 2015 *Adv. Theor. Math. Phys.* **19** 507–530 (*Preprint* `1206.6598`)

[45] Gralla S E and Zimmerman P 2018 *Class. Quant. Grav.* **35** 095002 (*Preprint* `1711.00855`)

[46] Gralla S E and Zimmerman P 2018 *JHEP* **06** 061 (*Preprint* `1804.04753`)

[47] Dias O J C, Godazgar M and Santos J E 2015 *Phys. Rev. Lett.* **114** 151101 (*Preprint* `1501.04625`)

[48] Vasil G, Lecoanet D, Burns K, Oishi J and Brown B 2018 *arXiv e-prints* arXiv:1804.10320 (*Preprint* `1804.10320`)

[49] Breuer R A, Ryan M P J and Waller S 1977 *Proceedings of the Royal Society of London Series A* **358** 71–86

[50] Press W H and Teukolsky S A 1973 *Astrophys. J.* **185** 649–674

[51] Bezanson J, Edelman A, Karpinski S and Shah V B 2017 *SIAM review* **59** 65–98 URL `https://doi.org/10.1137/141000671`

[52] RalphAS 2022 Genericschur, v0.5.2 `https://github.com/RalphAS/GenericSchur.jl` URL `https://github.com/RalphAS/GenericSchur.jl`

[53] Anderson E, Bai Z, Bischof C, Blackford S, Demmel J, Dongarra J, Du Croz J, Greenbaum A, Hammarling S, McKenney A and Sorensen D 1999 *LAPACK Users' Guide* 3rd ed (Philadelphia, PA: Society for Industrial and Applied Mathematics) ISBN 0-89871-447-8 (paperback)